Science Advances

AAAS

advances.sciencemag.org/cgi/content/full/3/5/e1700298/DC1

Supplementary Materials for

Global increase in replication fork speed during a $p57^{KIP2}$-regulated erythroid cell fate switch

Yung Hwang, Melinda Futran, Daniel Hidalgo, Ramona Pop, Divya Ramalingam Iyer, Ralph Scully, Nicholas Rhind, Merav Socolovsky

Published 26 May 2017, *Sci. Adv.* **3**, e1700298 (2017)
DOI: 10.1126/sciadv.1700298

The PDF file includes:

Other Supplementary Material for this manuscript includes the following:
(available at advances.sciencemag.org/cgi/content/full/3/5/e1700298/DC1)

- data file S1 (Microsoft Excel format). Spreadsheet containing the data set for the DNA combing experiment in Fig. 6.
- Image files (.pdf format)

Fig S1

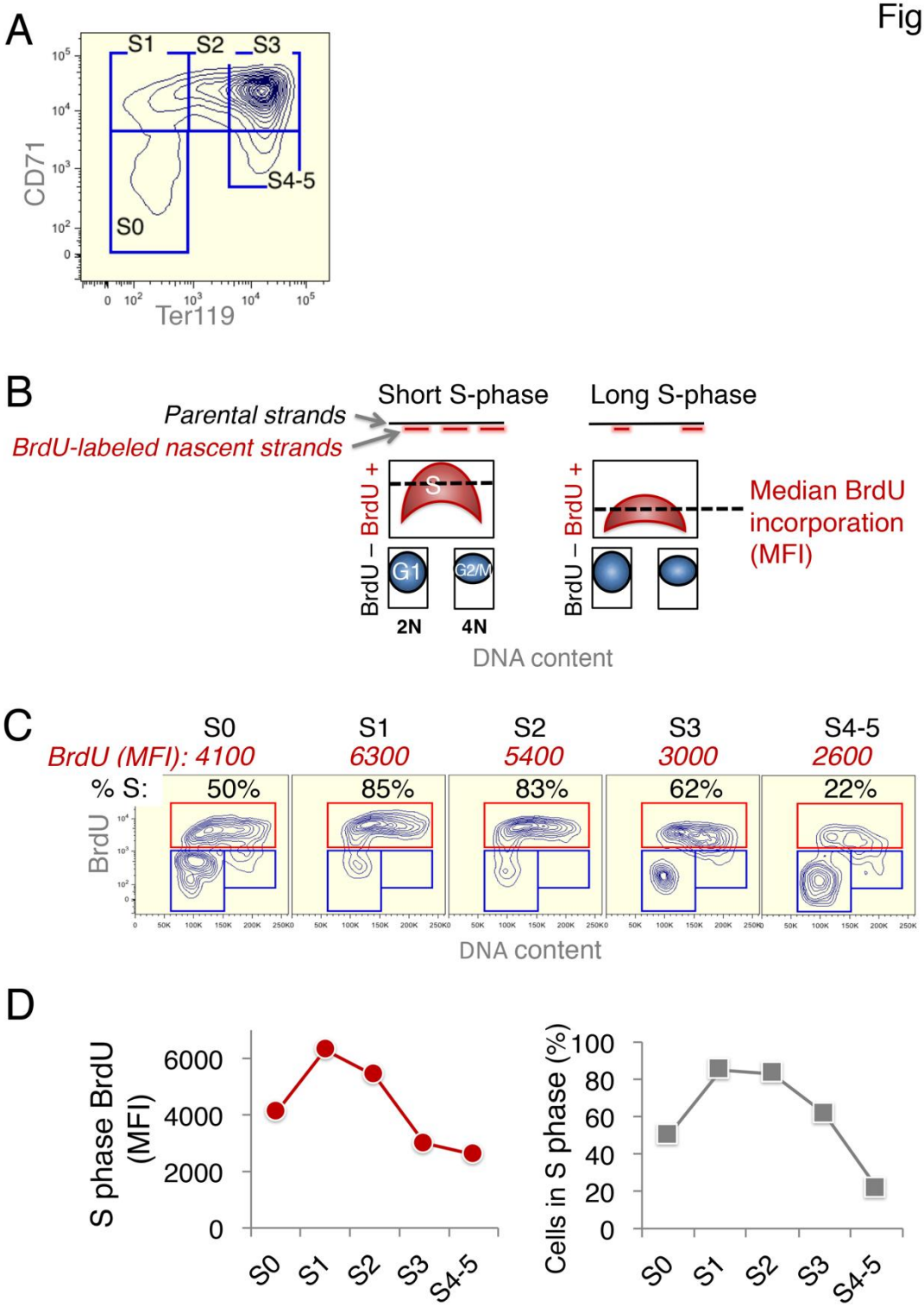

fig. S1. The transition from self-renewal to differentiation at S0/S1 is associated with a transient increase in intra–S-phase DNA synthesis rate. (**A**) Flow-cytometric profile of the fetal liver at embryonic day 13.5 (E13.5), divided into subsets S0 to S5 based on cell surface expression of CD71 and Ter119. Cells expressing non-erythroid markers were depleted prior to analysis as described (*23*). (**B**) Schematic illustrating the measurement of intra-S phase DNA synthesis rate using BrdU incorporation rate. All cells are subjected to the same 30’ BrdU pulse. Cells in S phase during the pulse incorporate BrdU into nascent DNA, becoming BrdU-positive.

Cells in which S phase is shorter replicate their genome faster, so that the total length of BrdU-labeled nascent DNA is longer than in cells with a slower S phase. The amount of BrdU incorporated into S phase cell populations may be measured as the median fluorescence intensity of the BrdU signal (BrdU MFI) in BrdU+ cells and is proportional to the median intra-S phase DNA synthesis rate. (**C** and **D**) Cell cycle status of fetal liver subsets S0 to S5. (C) shows flow cytometric profiles, (D) shows quantitation of the same data. A pregnant female mouse was pulsed in vivo with BrdU for 30' before harvesting fetal livers. Shown is an example of a single fetal liver, from the same embryo illustrated in (A). Cells were sorted digitally into subsets S1 to S5. The number of S phase cells and BrdU MFI were measured for each subset. The data are similar to data from pooled fetal livers published previously.

Fig S2

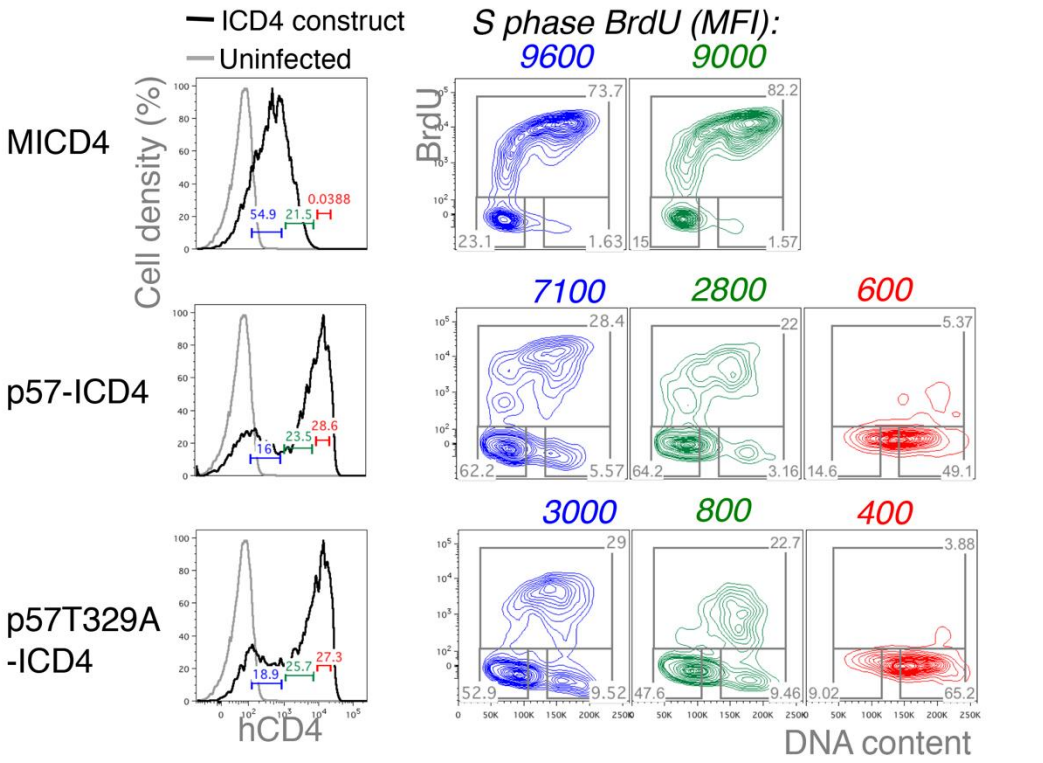

fig. S2. p57^{KIP2} exerts dose-dependent inhibition of DNA synthesis within S-phase cells. See also Fig. 2F. Experiment as described in Fig. 2F. Shown are 3 hCD4 gates for each of the transduced constructs, with corresponding cell cycle analysis. BrdU MFI is noted in italics above each plot.

Fig S3

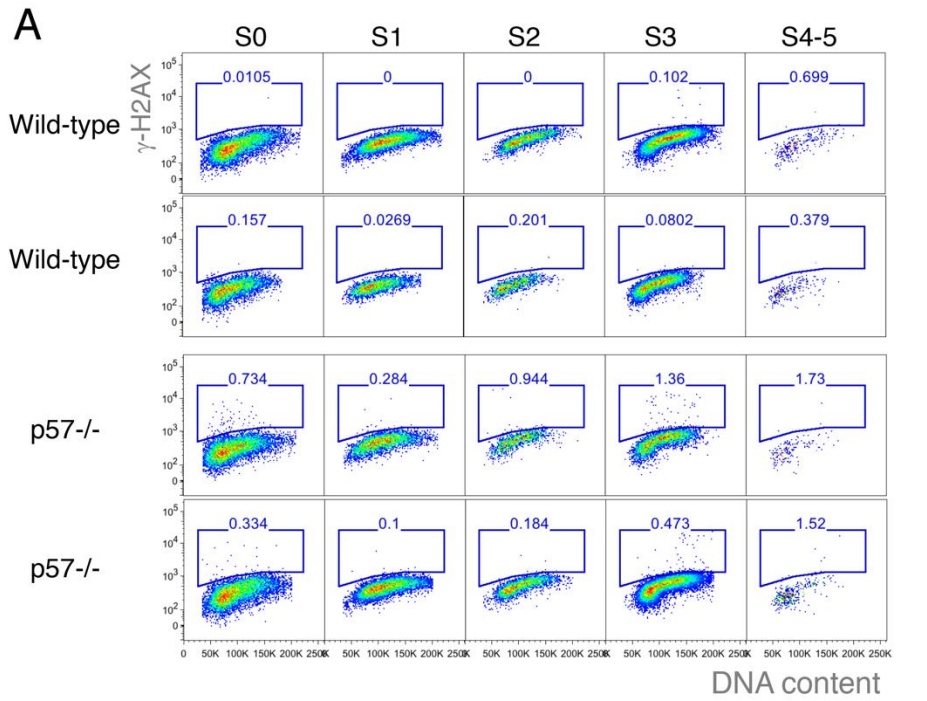

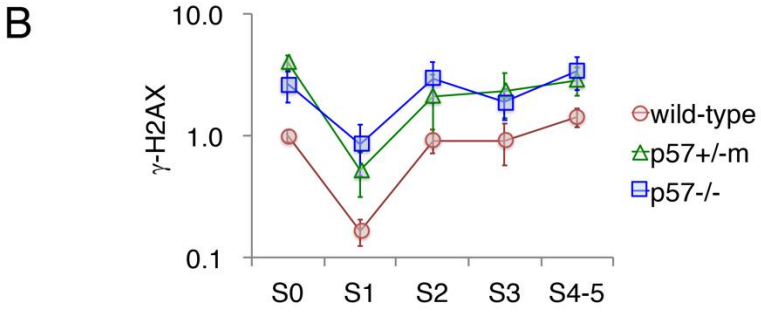

fig. S3. Increased γH2AX in p57^{KIP2}-deficient fetal liver. See also Fig. 4C-F. (**A**) Freshly explanted fetal livers of p57^{KIP2} -deficient embryos and wild-type littermates were labeled with an antibody against γ-H2AX. DNA content was measured using 7AAD. Representative examples are shown for littermate embryos for each of subsets S0 to S5. (**B**) Data summary for 71 embryos, experiment as described in (A). γ-H2AX levels are expressed relative to the mean γ-H2AX signal in wild-type S0 cells of each litter. Differences between p57^{KIP2} –deficient embryos and wild-type littermates are significant (paired *t* test, p=0.005 and 0.025 for p57^{KIP2} -/- and p57^{KIP2} -/+^{m}, respectively).

Fig S4

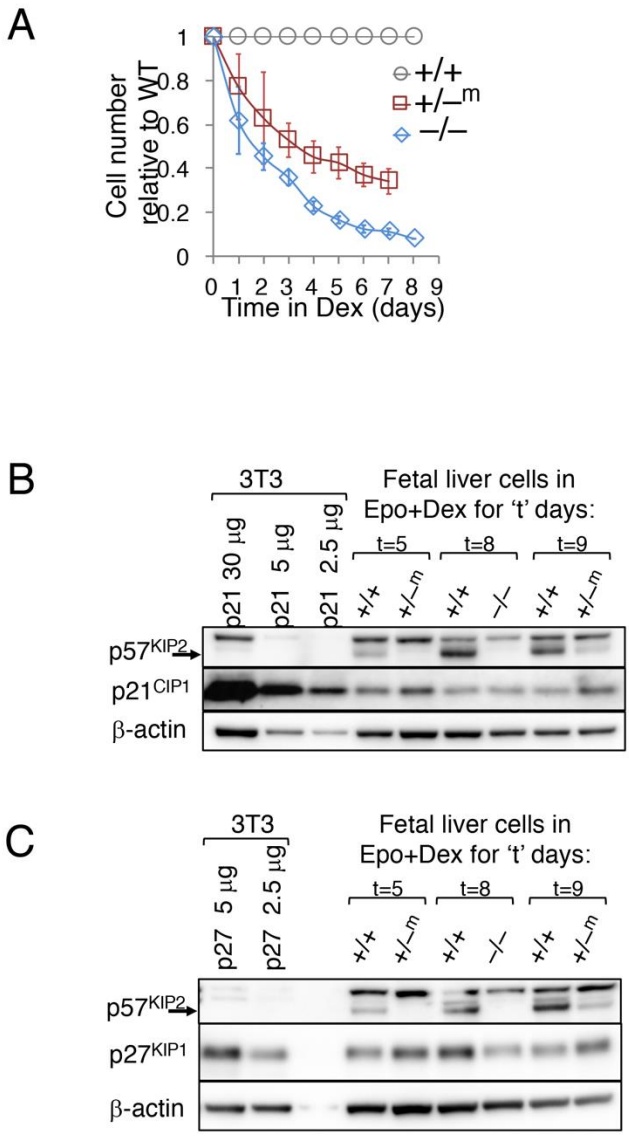

fig. S4. Analysis of p57^{KIP2}-deficient CFUe undergoing self-renewal in vitro. (**A**) p57^{KIP2}-deficient S0 cells fail to self-renew in vitro. Data as in Fig. 5D, but cell number is normalized to the respective wild-type cell number in each experiment. (**B**) and (**C**) Western blots showing no consistent compensatory upregulation of either p21^{CIP1} (B) or p27^{KIP1} (C) during 9 days of Dex-dependent S0 CFUe expansion in vitro. Control 3T3 cells were transduced with empty vector, or with vectors encoding either p21^{CIP1} or p27^{KIP1}. Low levels of the p57^{KIP2} protein in p57^{KIP2} +/-^{m} cells accumulate with increasing time of culture in self renewal medium (Epo + Dex).

Fig S5

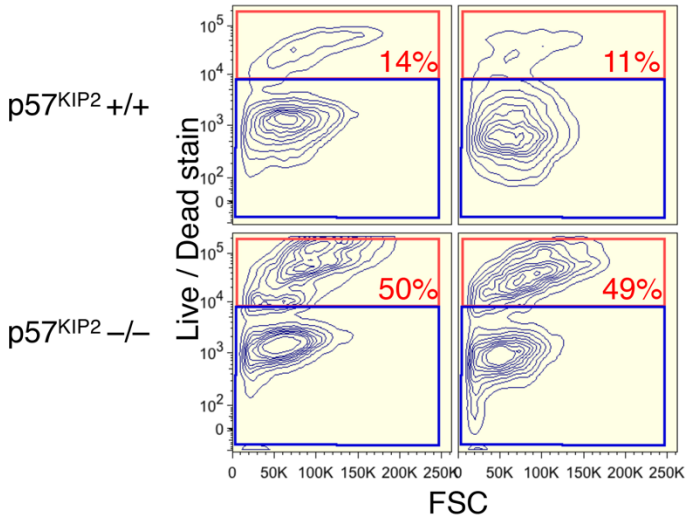

fig. S5. Increased cell death in p57$^{KIP2-/-}$ S0 CFUe during self-renewal in vitro. Cell death (upper gate, red) was measured by staining with the 'Live/Dead' reagent (Invitrogen), in cells undergoing Dex-dependent self-renewal in vitro. Two representative cultures of p57^{KIP2} -/- fetal livers are compared with two cultures of fetal livers from wild-type littermates, on day 4 of culture.

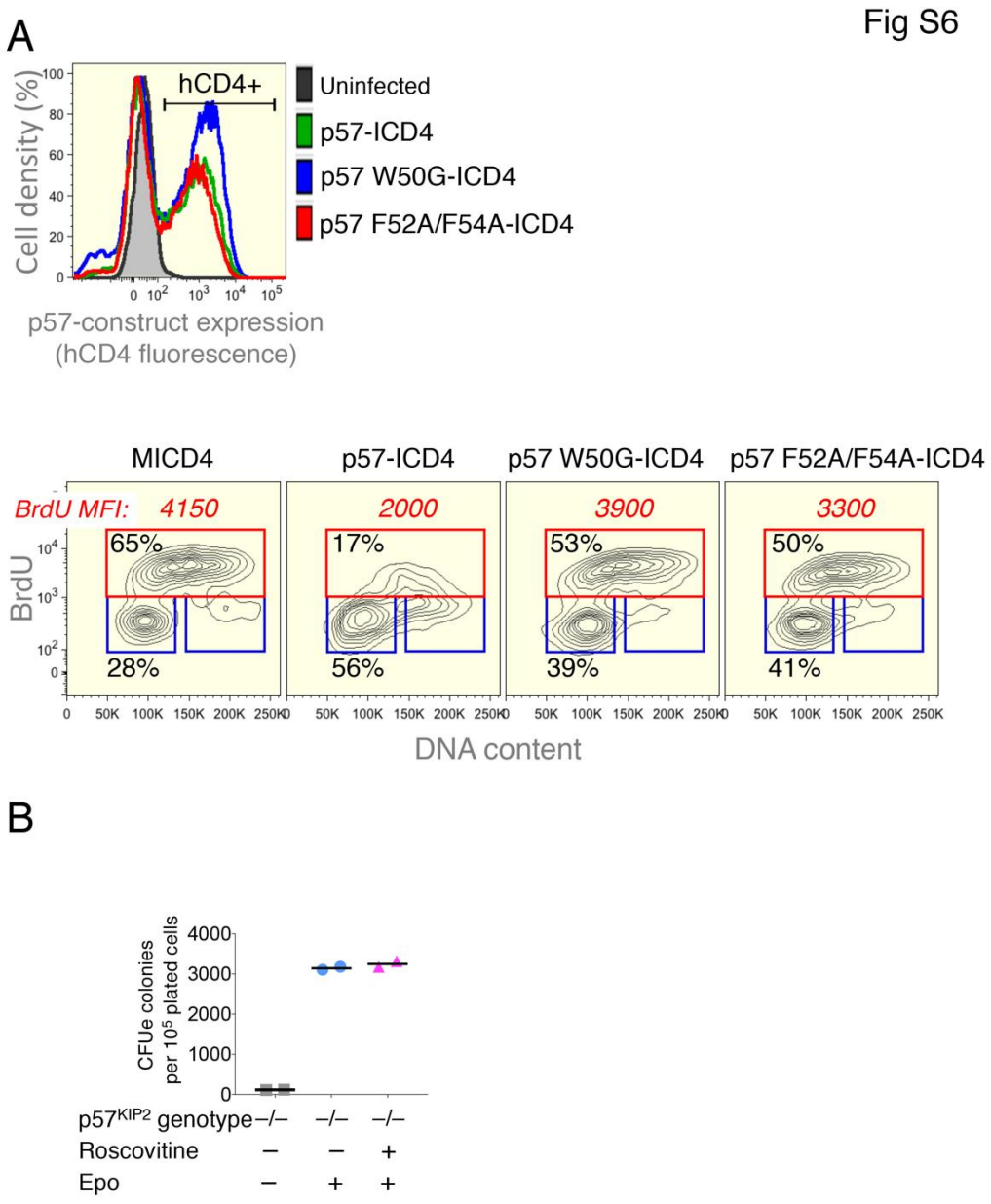

fig. S6. CFUe self-renewal requires the CDK-binding and inhibition functions of $p57^{KIP2}$. (**A**) Upper panel: S0 cells were transduced with wild-type $p57^{KIP2}$ or with the indicated $p57^{KIP2}$ mutants. The hCD4 reporter fluorescence identifies transduced cells. Lower panels: Cell cycle status, including intra- S phase DNA synthesis rate (BrdU MFI in the red gate, in red italics), for S0 cells that were transduced with the indicated constructs. Cell cycle analysis was done 15 hours post transduction. MICD4= 'empty' vector expressing only IRES-hCD4. (**B**) Analysis of CFUe potential in Dex-dependent self-renewal cultures of $p57^{KIP2}$ -/-cells treated with roscovitine (See Fig. 5I). On day 11 of culture, cells amplified in the presence or absence of roscovitine were plated at 10^5 cells per dish in Epo-containing semi- solid medium. The number of CFUe colonies formed per dish was scored 72 hours following plating. This analysis shows that the CFUe colony forming potential of roscovitine treated cells is similar to that of untreated cells (data are means of

two duplicates per conditions). Therefore, the increased cell number in roscovitine- treated $p57^{KIP2}$ -/- cultures (See Fig. 5I) reflects a genuine increase in CFUe self-renewal.

Fig S7

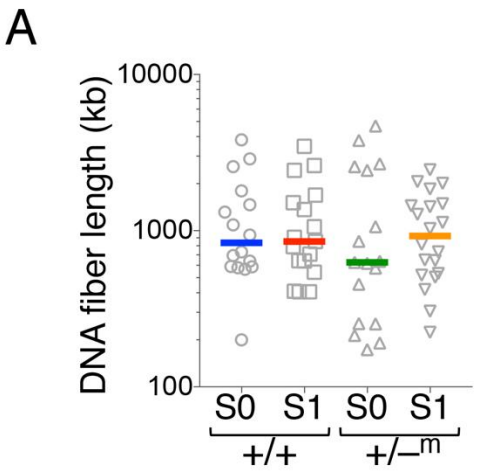

p57KIP2 genotype	+/+	+/+	+/–m	+/–m
	S0	S1	S0	S1
n	17	18	18	21
mean fiber length (kb)	1266	1172	1257	1042
SD	980	871	1363	653
Sum of all fiber lengths (kb)	21528	21107	22622	21888

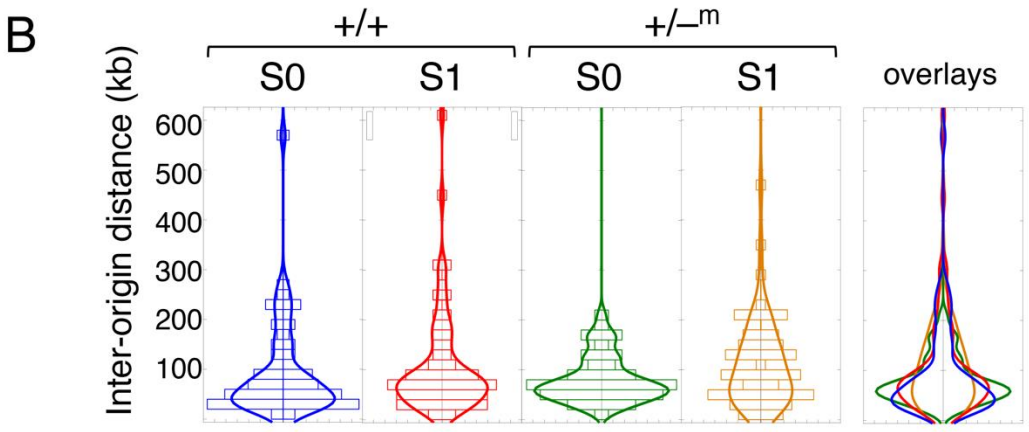

fig. S7. DNA combing analysis of freshly explanted fetal livers from wild-type and p57$^{KIP2+/-m}$ embryos associated with the experiment in Fig. 6. (**A**) Scatter plots for inter-origin distance distributions, same data as in Fig. 6C. (**B**) Violin plots for the DNA fiber lengths used in the experiment shown in this figure and in Fig. 6. The table shows total number, mean, standard deviation and sum of all analyzed DNA fibers for each cell type.

Fig S8

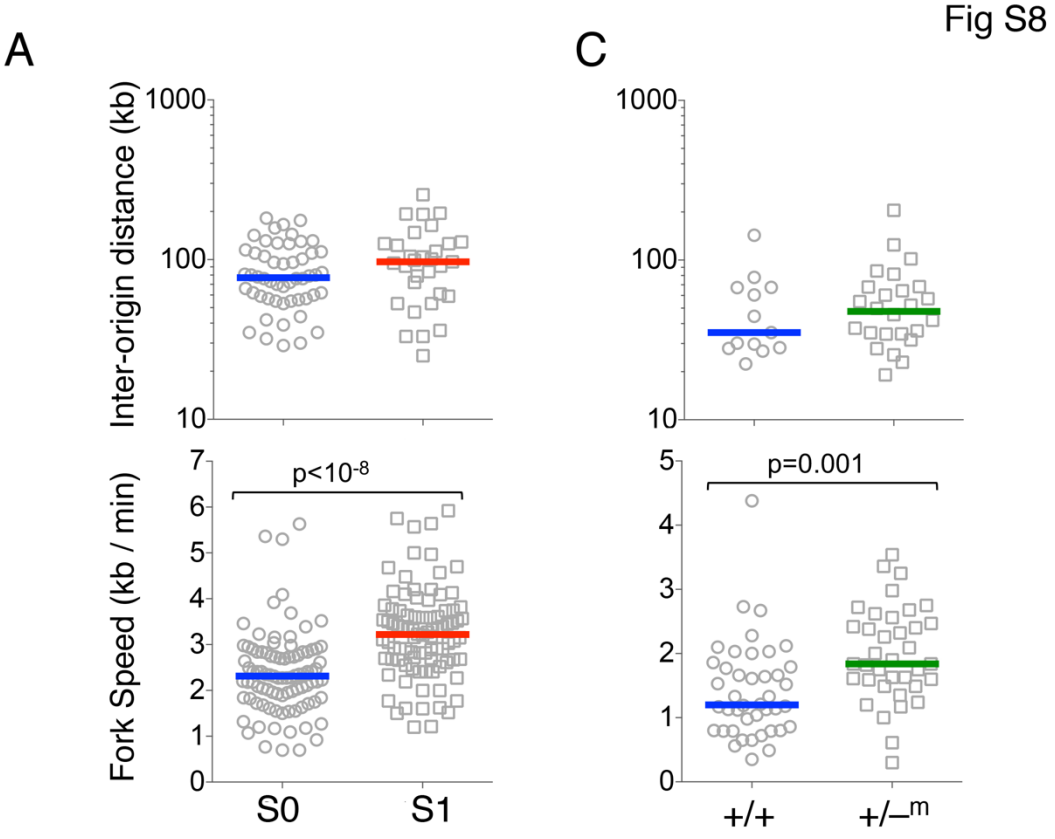

B

	S0 Subset	S1 Subset
n	52	57
Sum of all fiber lengths (Mb)	20.5	19.2
Median fiber length (kb)	360	369
Total number of forks	293	211
Total number of origins	113	80

fig. S8. DNA combing experiments. (**A**) DNA combing analysis of freshly explanted wild-type fetal liver from the Balb/C mouse strain. This is an independent experiment from the one presented in Fig. 6 and fig. S7. Experimental design as described in Fig. 6A. A total of 90 (S1) and 92 (S0) forks that moved throughout the IdU pulse are compared. (**B**) DNA fiber statistics for the experiment illustrated in (A). (**C**) A DNA combing experiment of Dex-dependent cultures in which S0-derived CFUe undergo self-renewal. Two cultures, from wild-type and $p57^{KIP2+/-m}$ littermates, were analyzed on day 5 of the culture. A total of 8Mb of DNA were examined, mean fiber length= 384kb.

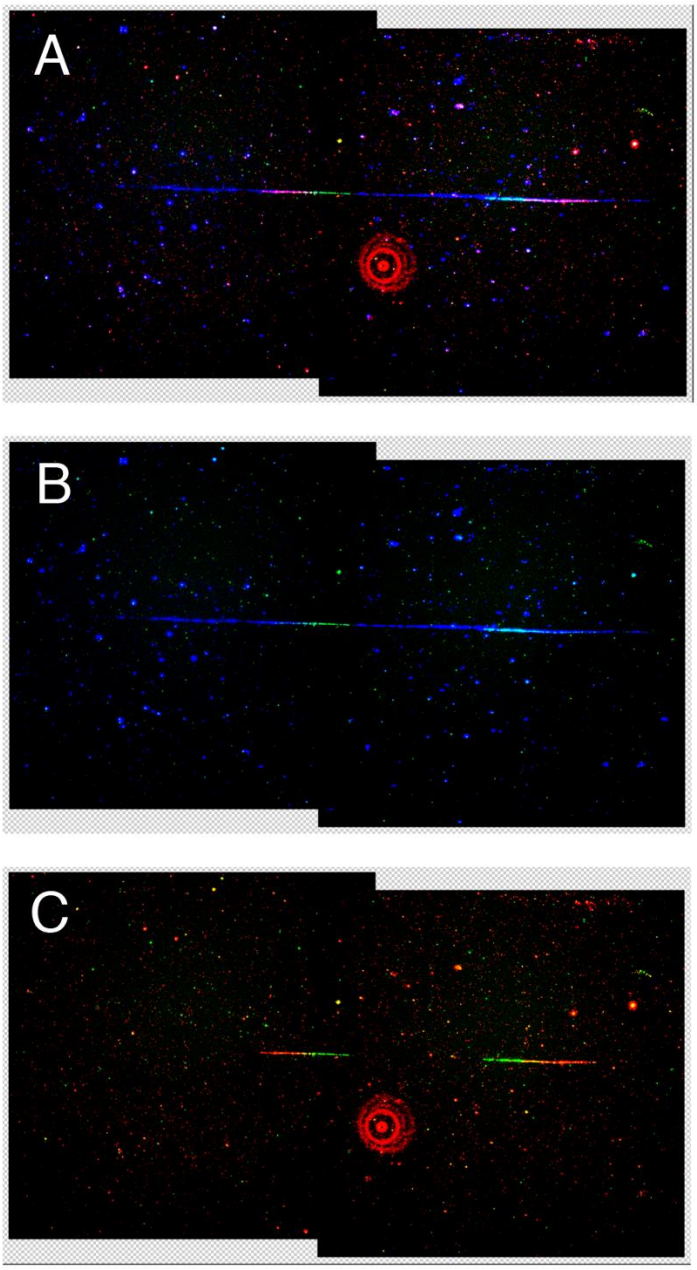

fig. S9. DNA combing: Example of fluorescence image file used for scoring data. A DNA fiber spanning two partly overlapping microscope fields of view. Three exposures were taken for each field, separately capturing green, red and blue fluorescence. The three fluorescence images for each field were digitally merged into a single file. The two merged files, each corresponding to a field of view, were then aligned to reproduce the full length of the fiber in a composite image shown above. In **A**, **B** and **C**, are shown either all colors, or just two of the three colors in the image. Average image files used for the DNA combing data were composites of up to 30 microscope fields.